Long-range interlayer-coupled magnetization reversal mediated by the antiferromagnetic layer in Py/FeMn/CoFe trilayers

Ki-Yeon Kim,[1,*] Ji-Wan Kim,[2] Hyeok-Cheol Choi,[3] A. Teichert,[4,5,6] Chun-Yeol You,[3,†] Sungkyun Park,[7] Sung-Chul Shin,[2] and Jeong-Soo Lee[1]

[1]*Neutron Science Division, Korea Atomic Energy Research Institute, Daejeon 305-353, Republic of Korea*

[2]*Department of Physics and Center for Nanospinics of Spintronic Materials, Korea Advanced Institute of Science and Technology, Daejeon 305-701, Republic of Korea*

[3]*Department of Physics, Inha University, Incheon 402-751, Republic of Korea*

[4]*Helmholtz Zentrum Berlin für Materialien und Energie, Hahn-Meitner-Platz1, D-14109 Berlin, Germany*

[5]*Institute voor Kern-en Stralingsfysica and INPAC, K. U. Leuven, Celestijnenlaan 200D, B-30001 Leuven, Belgium*

[6]*Laboratorium voor Vaste-Stoffysica en Magnetisme and INPAC, K. U. Leuven, Celestijnenlaan 200D, B-30001 Leuven, Belgium*

[7]*Department of Physics, Pusan National University, Pusan 609-735, Republic of Korea*

(Received 12 April 2011; revised manuscript received 26 July 2011; published 5 October 2011)

With a combination of vector magneto-optical Kerr effect magnetometry and polarized neutron reflectometry, the detailed magnetization reversal mechanism of the exchange-biased Py(30-nm)/FeMn[t_{AFM} = (0–30)-nm]/CoFe(30-nm) trilayers was studied. We found that Py/FeMn(15-nm) and FeMn(15-nm)/CoFe bilayers show completely different magnetization reversal modes, whereas they become very similar to each other in the corresponding Py/FeMn/CoFe trilayers. This is convincing evidence that the 15-nm FeMn layer mediates the magnetization reversal behaviors of both Py and CoFe layers through interlayer exchange bias coupling. Furthermore, magnetization reversal of Py and CoFe layers are decoupled for $t_{AFM} = 30$ nm, indicating that the exchange length the magnetization reversal between two adjacent ferromagnetic layers is correlated over is less than 30 nm. This is in reasonable agreement with the theoretically predicted domain-wall width such as 28 nm for the polycrystalline FeMn/Co bilayer and 50 nm for the perfect $Fe_{50}Mn_{50}$ crystal.

DOI: 10.1103/PhysRevB.84.144410 PACS number(s): 75.30.Et, 75.50.Ee, 75.60.Jk

I. INTRODUCTION

The exchange coupling between a ferromagnetic (FM) and an antiferromagnetic (AFM) thin films across their common interface manifests itself as breaking the symmetry of the magnetic hysteresis (M-H) loop and shifting the loop by an exchange bias field (H_E) away from $H = 0$ after field cooling from above the Néel temperature or sample deposition under the influence of an applied field.[1] Other important aspects of the exchange coupling include coercivity (H_C) enhancement, asymmetric reversal mechanisms, training effects, and noncollinear magnetic anisotropies.[2–6] In addition to being of fundamental interest, these properties have found applications in spintronic devices such as a magnetic random access memory and a magnetic-field sensor based on giant magnetoresistance or tunnel magnetoresistance spin valves due to their advantage of pinning the FM magnetization effectively in magnetic multilayers.[7,8]

Although the exchange bias was originally considered as the pure interface effect between FM and AFM layers, Gökemeijer *et al.*[9] reported that exchange coupling is not a short-range interaction between nearest-neighbor FM and AFM spins, but a long-range one in Py/spacer/CoO trilayers with Ag, Au, and Cu as spacer materials. The coupling strength shows exponential decay and the coupling length is surprisingly extended to 5 nm, which is much longer than that for simple atomic exchange coupling. Furthermore, a different dependence of the exchange bias field on the spacer layer thickness has been observed experimentally in various FM/spacer/AFM systems such as IrMn/spacers (Cu, Ag, Au, Pd, Ru, Al, Ti)/Co,[10] Co/(Cu, Au)/CoO,[11,12] (Pt/Co) multilayer/Pt/FeMn,[13] and FeNi/Cu/FeMn.[14] These observations indicate that the long-range nature of exchange bias is not so simple. In order to reveal the underlying physics of exchange bias, deeper investigations are required.

Besides the FM/spacer/AFM trilayer, the FM/AFM/FM trilayer would be a very good model structure to explore the underlying physics of exchange bias.[15–18] Yang and Chien[16] claimed that the spiral spin structure was observed in the oppositely exchange-biased Py/FeMn(111)/Co trilayers from a vibrating sample magnetometer and the spiral length was found to be 9 nm. Nam *et al.*[17] reported that an antiferromagnetic FeMn layer mediates exchange bias fields between the bottom CoFe/FeMn and top FeMn/CoFe interfaces in the CoFe/FeMn(111)/CoFe trilayers in which an AFM thickness t_{AFM} ranges from 5 to 10 nm. These results are likely to indicate the long-range exchange bias coupling across the AFM layer between two neighboring FM layers in the FM/AFM/FM trilayers. However, there has been no report so far on the interlayer-coupled magnetization reversal behavior between two FM/AFM interfaces with varying AFM thickness in the exchange-biased FM/AFM/FM trilayers. We have studied the details of the layer- and vector-resolved magnetization reversal mechanism in Py(bottom)/FeMn(t_{AFM})/CoFe(top) trilayers with $t_{AFM} \leqslant 30$ nm by measuring a longitudinal magneto-optical Kerr effect (MOKE) along with polarized neutron reflectivity (PNR). We found convincing evidence that the magnetization reversal of both Py and CoFe layers is coupled through the 15-nm FeMn layer in the Py/FeMn/CoFe trilayers and the exchange length along which the polycrystalline FeMn layer mediates the magnetic reversal is less than 30 nm.

II. EXPERIMENT

Magnetic trilayers consisting of Py(30 nm, bottom)/FeMn(t_{AFM})/CoFe(30 nm, top) with $t_{AFM} = 0, 2, 5, 7, 9, 12, 15$, and 30 nm were grown on optically transparent glass substrates at an ambient temperature using a dc magnetron sputtering at an Ar working pressure of 1.5 mTorr. The thickness unit in parentheses is hereinafter in nanometers. The base pressure was kept low at 10^{-9} Torr. In addition, Py(30)/FeMn(15) and FeMn(15)/CoFe(30) bilayers and 30-nm Py and CoFe single layers were prepared as reference samples. A Ta(5) underlayer for trilayers and a Ta(5)/Cu(5) underlayer for bilayers were incorporated to promote a FeMn(111) texture, which is essential for exchange bias, and a Ta(5) capping layer was used as a passivation layer.[19] A magnetic field of 300 Oe was applied along the sample plane during deposition to induce the exchange anisotropy. Details of a sample preparation can be found elsewhere.[20] The film thickness and growth texture were characterized by low-angle x-ray reflectivity and high-angle $\theta/2\theta$ x-ray diffraction (not shown here).

In order to measure separately the longitudinal ($M_{\parallel}$) and transverse ($M_{\perp}$) magnetization components with layer selectivity, we employed both the vector MOKE and PNR. It is well known that both $M_{\parallel}$-H and $M_{\perp}$-H loops from the vector MOKE can be achieved by rotating both a sample and magnet by 90° and fixing the others with *s*-polarized light incident on both the front of the sample and the back of the substrate.[21,22] The schematic view of the vector MOKE setup is shown in Fig. 1(a) and a detailed description can be found elsewhere.[23] To ensure layer selectivity in our trilayers as shown in Fig. 1(b), we prepared samples on a transparent substrate and optimized each layer thickness of Py, CoFe, and Ta by taking into account the skin depth of 3*d* transition metals, which is typically about 25–30 nm. Our vector MOKE setup makes it possible to determine the magnetization reversal behavior of each FM layer in the exchange-bias Py/FeMn/CoFe trilayers with layer selectivity. As a complement to the MOKE, PNR has proven to have the unique advantage of distinguishing different magnetization reversal modes with layer selectivity in magnetic thin films and multilayers.[24,25] The specular PNR experiment was performed with a V6 neutron reflectometer at Helmholtz Zentrum Berlin, Germany, which uses a cold neutron beam with a wavelength λ of 0.466 nm. A schematic view and the reflection geometry of the V6 reflectometer are shown in Figs. 1(c) and 1(d), respectively; further detailed information can be found elsewhere.[26] For specular PNR where an incidence angle is equal to a reflected angle, there are two non-spin-flip (NSF) and two spin-flip (SF) reflection cross sections. The cross sections for the NSF reflection, where the neutron's polarization is conserved after reflection, e.g., from spin up to spin up, are sensitive to the chemical structure and the difference between R^{++} and R^{--} reflectivities ($R^{++} - R^{--}$) is proportional to $M_{\parallel}$. The first (second) superscript in R^{++} and R^{--} denotes the spin-polarization direction of incident (reflected) neutrons with respect to magnetization projected on an applied field. In contrast, the cross sections for the SF reflection, where neutron polarization is changed after reflection, e.g., from spin up to spin down and vice versa, are sensitive to the $M_{\perp}$ in the sample plane.[24,25] Non-spin-flip and SF reflectivities were measured as a function of the wave-vector transfer $Q = 4\pi \sin\theta/\lambda$ by varying the incidence angle θ up to 2.1° at a saturation field. For a specific Q where $R^{++} - R^{--}$ measured at a saturation field is maximized, NSF (I^{++}, I^{--}) and SF (I^{+-}, I^{-+}) intensities were scanned by sweeping an applied magnetic field. Two important points should be noted. First, the normalized spin asymmetry (NSA) $(I^{++} - I^{--})/(I^{++} + I^{--})$, which is defined by the NSF intensity, allows us to find an M-H loop. Second, SF intensities should vanish at saturation fields and could distinguish domain-wall motion (vanishing $M_{\perp}$) from rotation motion (nonvanishing $M_{\perp}$) during the magnetization reversal process around left (H_{LC}) and right (H_{RC}) coercivities.[27]

III. RESULTS AND DISCUSSION

The representative vector MOKE hysteresis loops of Py(30)/FeMn(15) and FeMn(15)/CoFe(30) bilayers and a Py(30)/FeMn(15)/CoFe(30) trilayer are displayed in Figs. 2(a)–2(c), respectively. Interestingly, a nonvanishing $M_{\perp}$ was observed only in the Py/FeMn bilayer and not in the FeMn/CoFe bilayer. This indicates that the magnetic reversal occurs with an accompanying magnetization rotation in the Py/FeMn layer, while the magnetic reversal takes place only through domain-wall motion in the FeMn/CoFe bilayers. In contrast, it is revealed that the CoFe layer as well as the Py layer clearly shows a nonzero $M_{\perp}$-H loop in the corresponding Py/FeMn/CoFe trilayer [Fig. 2(c)]. This is clear evidence that the magnetization reversals of two exchange-biased FM layers are coupled through the 15-nm-thick FeMn layer. These nonzero $M_{\perp}$-H loops are observed in the exchange-biased Py/FeMn/CoFe loops with $t_{AFM} < 15$ nm. Yang and Chien[16] claimed that the length of the spiraling AFM spin structure is a minimum AFM domain-wall thickness (~9 nm) theoretically predicted to be proportional to $\sqrt{A_{AFM}/K_{AFM}}$, where A_{AFM} is the exchange stiffness constant and K_{AFM} is the magnetic anisotropy constant. However, their result is different from the calculated result of Ali *et al*. that a typical planar domain-wall width in the FeMn layer is estimated to be 28 nm for the FeMn/Co bilayer.[28] In contrast, a theoretical upper limit for the domain-wall width in the $Fe_{50}Mn_{50}$ perfect crystal is known to be about 50 nm.[29] Therefore, we expect that the exchange length of FeMn(111) texture along the direction normal to the film plane could be between 9 and 50 nm.

Besides magnetization reversal, exchange-bias fields should be different between bilayers and trilayers due to the interlayer exchange-bias coupling. Nam *et al*.[17] reported that the H_E of both CoFe layers is improved due to the magnetic coupling between two CoFe/FeMn and FeMn/CoFe interfaces sharing a FeMn layer by combining the two CoFe/FeMn bilayers into a symmetric CoFe/FeMn(5–10)/CoFe trilayer. In our case, the H_E are −8.7 and −44.1 Oe and the H_C are 37.2 and 7.9 Oe from $M_{\parallel}$-H loops of the FeMn(15)/CoFe(30) and Py(30)/FeMn (15) bilayers, respectively, as shown in Figs. 3(a) and 3(b). Meanwhile, the H_E of a corresponding trilayer are −5.2 Oe (CoFe) and −32.3 Oe (Py), which are decreased by 30%–40% compared with the H_E of bilayers, as shown in Fig. 2(c). This is reminiscent of exchange-bias coupling between Py and CoFe layers across a FeMn intervening layer in a Py/FeMn(15)/CoFe trilayer.

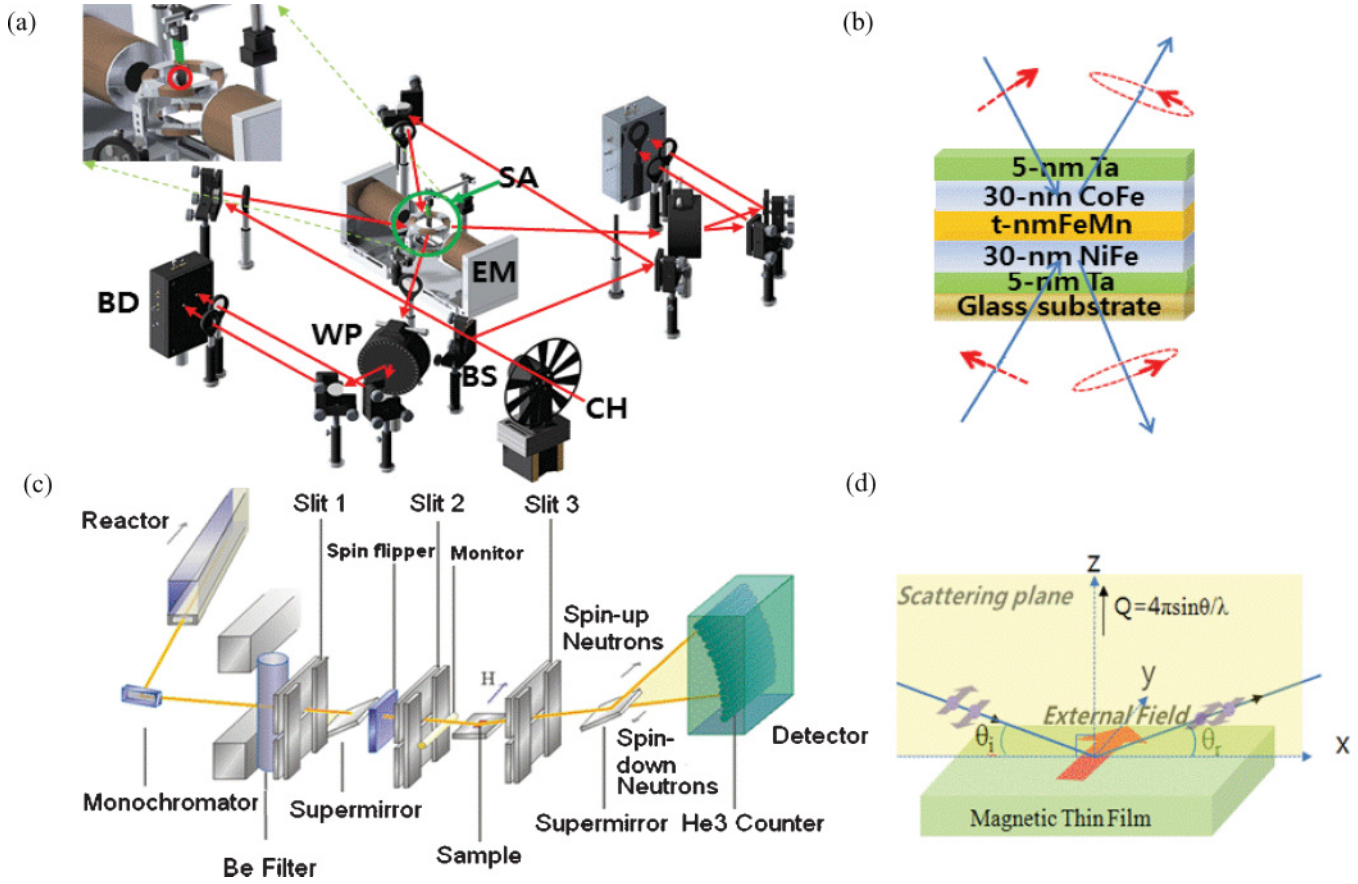

FIG. 1. (Color online) (a) Experimental setup of the vector magneto-optical Kerr effect magnetometer where BD, WP, SA, EM, BS, and CH stand for balanced detector, Wollaston prism, sample, electromagnet, beam splitter, and chopper, respectively. The inset shows the magnified picture of a sample region. (b) Typical sample structure. (c) Schematic view of the V6 polarized neutron reflectometer at Helmholtz Zentrum Berlin, Germany[26] (d) Specular reflection geometry of polarized neutrons incident on a sample plane.

To corroborate the magnetization reversal behavior of Py(30)/FeMn(15)/CoFe(30) trilayers as well as Py(30)/FeMn(15) and FeMn(15)/CoFe(30) bilayers, we have performed spin-dependent neutron intensity measurements by sweeping a magnetic field between −150 and 150 Oe along the deposition field. It should be noted that when a magnetic field was applied along the negative field axis of the *M-H* loop, we rotated a sample by 180° in the film plane without reversing the direction of the applied field with respect to the guide field due to neutron beam depolarization. Magnetic-field scan data of NSF and SF intensities of Py/FeMn and FeMn/CoFe bilayers and a Py/FeMn/CoFe trilayer are shown in Figs. 3(b), 3(d), and 3(f). From these data, NSA is obtained as a function of an applied field and is plotted along with the MOKE $M_{\parallel}$-H loop as shown in Figs. 3(a), 3(c), and 3(e).

In the case of the Py/FeMn bilayer as shown in Fig. 3(a), the $M_{\parallel}$-H hysteresis loops from the NSA and MOKE are very similar to each other. Furthermore, the H_E are −46.0 Oe for PNR and −45.9 Oe for the MOKE, which coincide with each other. The pronounced peaks appear in SF intensities around the left ($H_{\mathrm{LC}} = -52.7$ Oe) and right coercivities ($H_{\mathrm{RC}} = -39.3$ Oe), in which case $I^{++} = I^{--}$. The SF peak intensity is less than the NSF intensity by one order of magnitude. These results indicate that magnetization reversal accompanies domain-wall propagation as well as magnetic rotation in the Py/FeMn bilayer. It is worth noting that the MOKE intensity between left and right coercivities is very different in the transverse component of the Py layer in Figs. 2(a) and 2(c). These asymmetric hysteresis loops have been reported in a number of exchange-bias systems from various magnetometry methods and are found to be related to the asymmetric magnetization reversal induced by the interfacial exchange coupling between FM and AFM spins.[3,30–32] However, it is also known that especially for the magnetization reversal measurement using MOKE magnetometry, the second-order MOKE can lead to the asymmetric hysteresis loops that are not observed using other magnetometry methods.[33] Therefore, it is necessary to distinguish the second-order MOKE and asymmetric magnetic hysteresis induced by exchange bias.[34] From our PNR experiment on the same sample, it is likely that the magnetization reversal is not asymmetric between left and right coercivities because SF intensities are similar to each other at both coercivities, as shown in Fig. 3(b). The combination of the MOKE and PNR magnetometry could be a good combination for clarifying the detailed magnetization reversal. It should be kept in mind that this asymmetry has nothing to do with that two adjacent FM layers separated by

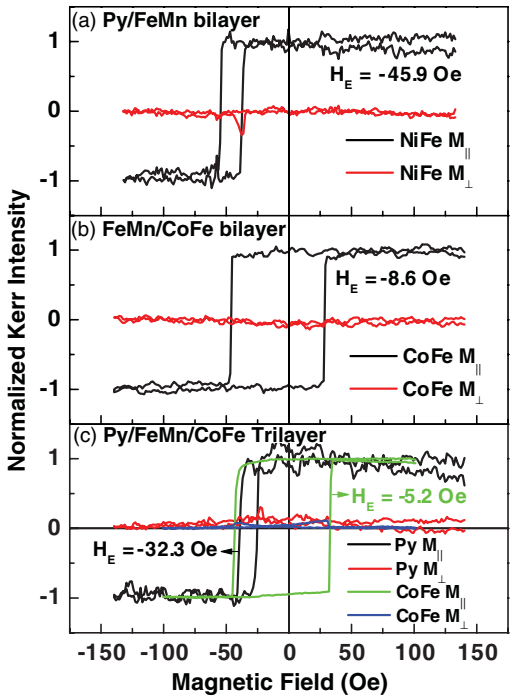

FIG. 2. (Color) Longitudinal ($M_{\parallel}$-H, black) and transverse ($M_{\perp}$-H, red) loops of the (a) Py(30)/FeMn(15) and (b) FeMn(15)/CoFe(30) bilayers and longitudinal ($M_{\parallel}$-H, black; $M_{\perp}$-H, green) and transverse ($M_{\parallel}$-H, red; $M_{\perp}$-H, blue) loops of the (c) Py(30)/FeMn(15)/CoFe(30) trilayer, respectively.

an AFM layer affect magnetization reversal with respect to each other.

The $M_{\parallel}$-H hysteresis loops and exchange-bias fields from the NSA and MOKE of the FeMn/CoFe bilayer as shown in Fig. 3(c) are also similar to each other. It should be mentioned that there are clear differences between I^{+-} and I^{-+} in the field range less than each coercivity before the polarization correction (not shown here). If our field scan data are calibrated for polarization efficiency according to Wildes's method,[35] two SF intensities become equal to each other. It was found that this difference is attributed to the different polarization efficiencies of the analyzer for analyzer-reflected and analyzer-transmitted neutrons. The polarization correction method of the V6 reflectometer can be found in the Appendix. After the polarization correction, there are no SF intensities around the left ($H_{\mathrm{LC}} = -51.9$ Oe) and right coercivities ($H_{\mathrm{RC}} = 28.8$ Oe). This indicates that magnetization reversal takes place through domain-wall nucleation and propagation without magnetic rotation. These results are in good agreement with the corresponding MOKE hysteresis loops in Fig. 2(b) as well. These apparently different magnetic reversal modes of the exchange-biased Py/FeMn and FeMn/CoFe layers give us an opportunity to study the interlayer magnetization reversal coupling between adjacent FM layers in FM/AFM/FM trilayers by varying the AFM layer thickness.

For the combined exchange-biased Py/FeMn(15)/CoFe trilayer, nonzero SF intensities at both H_{LC} and H_{RC} of the Py and CoFe layers are clearly observed as displayed in Fig. 3(f) and the SF intensities are less than the NSF intensities by an order of magnitude. These results demonstrate that

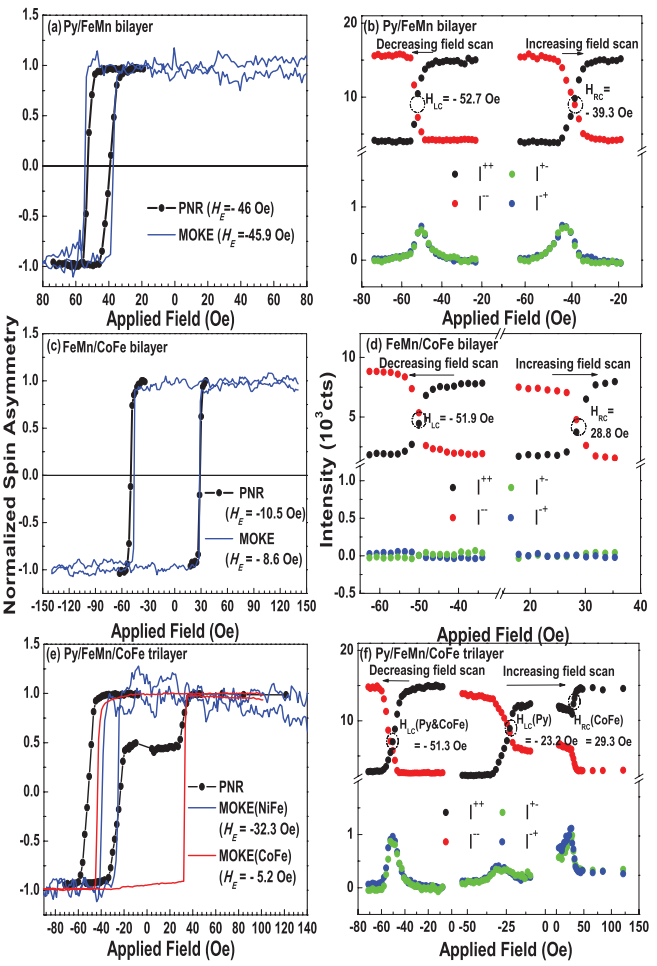

FIG. 3. (Color online) NSA $(I^{++} - I^{--})/(I^{++} + I^{--})$ as a function of an applied field along with the MOKE hysteresis loop of (a) an exchange-bias Py(30)/FeMn(15) bilayer, (c) an exchange-bias FeMn(15)/CoFe(30) bilayer, (e) an exchange-bias Py(30)/FeMn(15)/CoFe(30) trilayer, and (b), (d), and (f) the corresponding NSF (I^{++}, black; I^{--}, red) and SF (I^{+-}, green; I^{-+}, blue) intensity scan data.

magnetization reversal of Py has a strong influence on that of the CoFe layer across a thick FeMn layer and both of them proceed with magnetic reversal via a combination of magnetic rotation and domain-wall propagation. Although H_{LC} from the MOKE and NSA show different values [shown in Fig. 3(e)] and the reason for that is still unclear, it has nothing to do with magnetization reversal mode. Therefore, PNR results are in qualitative accord with the MOKE experimental results on the magnetization reversal behavior.

To examine the critical thickness by which the magnetization reversal of two FM layers separated by a common AFM layer is decoupled, both the $M_{\parallel}$-H and $M_{\perp}$-H loops of the Py and CoFe layers were measured in the exchange-biased Py/FeMn(30)/CoFe trilayer using our vector MOKE. As shown in Fig. 4, during reversal at H_{LC} and H_{RC}, $M_{\perp}$ were observed only at the Py layer and not at the CoFe layer. This indicates that magnetization reversal takes place via both magnetic rotation and domain-wall propagation in the exchange-biased Py layer, but only via nucleation and

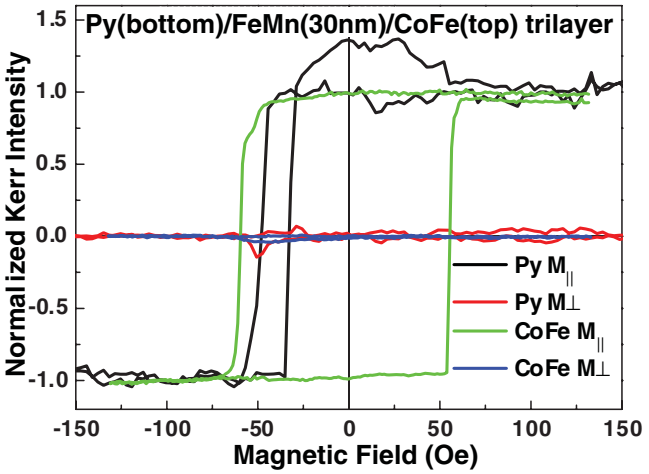

FIG. 4. (Color online) Longitudinal ($M_{\parallel}$-H, black) and transverse ($M_{\perp}$-H, red) loops of a Py layer and longitudinal ($M_{\parallel}$-H, green) and transverse ($M_{\perp}$-H, blue) loops of a CoFe layer in the exchange-bias Py(30)/FeMn(30)/CoFe(30) trilayer.

domain-wall propagation in the exchange-biased CoFe layer. This reveals that the magnetization reversals of the Py and CoFe layers are independent of each other for the case of $t_{\mathrm{AFM}} = 30$ nm, below which a polycrystalline FeMn(111) layer mediates magnetization reversal between adjacent FM layers. This exchange length experimentally obtained for the polycrystalline FeMn(111) layer is larger than Yang and Chien's result[16] but is in reasonable agreement with the theoretical upper limit of the domain-wall width (∼50 nm) for a perfect $Fe_{50}Mn_{50}$ crystal and the calculated value (28 nm) for the FeMn/Co bilayer.[28,29] Our experimental result is of fundamental importance in that an effective exchange length within the polycrystalline FeMn(111) layer can be quantitatively determined in the FM/AFM/FM trilayer. The H_E of Py is about 40.8 Oe, which is close to that of the Py/FeMn bilayer, but not to that of the CoFe layer. Because H_E tends to saturate after $t_{\mathrm{AFM}} = 10$ nm, we emphasize that using the magnetization reversal would better than H_E to study the interlayer coupling between adjacent FM layers separated by a thick AFM layer in our samples.

IV. CONCLUSION

We find compelling evidence that the magnetization reversals of two adjacent Py and CoFe layers are coupled through a thick FeMn layer up to 15 nm in the exchange-bias Py/FeMn/CoFe trilayers with a combination of layer- and vector-resolved magneto-optical Kerr effect magnetometry and polarized neutron reflectometry. In addition, the maximum coupling length for FeMn(111) is found to be less than $t_{\mathrm{AFM}} = 30$ nm. This is accordant with theoretically predicted values, such as 28 nm for polycrystalline FeMn(111) and 50 nm for crystalline FeMn(111). Our experimental approach and results clearly provide an alternative way to examine a long-range exchange-bias coupling via the magnetization reversal in FM1/AFM/FM2 trilayers.

ACKNOWLEDGMENTS

This work was supported by Nuclear R&D program, NRF (Grant Nos. 2010-0022040 and 2010-0023798), GPP (Grant No. K20703001300-09E0100-06910), NRL (Grant No. 2010-0019293), and NRF (Grant No. 2010-0018374) through the National Research Foundation of Korea.

APPENDIX: POLARIZATION CORRECTION OF THE V6 REFLECTOMETER

It is necessary to correct the raw PNR data by taking into account polarization efficiency contributions from an imperfect guide field, electromagnet, polarizer or analyzer, and spin flippers. Polarization correction was done based on the method given by Wildes,[35] but two points should be highlighted. First, the polarization correction method with flippers is given in a simple matrix form, but the polarizer and analyzer efficiencies are defined when they are configured to transmit spin-up neutrons, not spin-down neutrons. However, the polarizer and analyzer in the V6 reflectometer transmit spin-down neutrons and reflect spin-up neutrons. Therefore, their formula cannot be directly applicable to our field scan data and should be modified as follows:

$$[\Sigma] = [A][F_A][P][F_P][I'], \quad [\Sigma] = \begin{bmatrix} \Sigma^{++} \\ \Sigma^{+-} \\ \Sigma^{-+} \\ \Sigma^{--} \end{bmatrix}, \quad [I'] = \begin{bmatrix} I^{++} \\ I^{+-} \\ I^{-+} \\ I^{--} \end{bmatrix}, \quad [F_P] = \frac{1}{f_p} \begin{bmatrix} 1 & 0 & (f_p - 1) & 0 \\ 0 & 1 & 0 & (f_p - 1) \\ 0 & 0 & f_p & 0 \\ 0 & 0 & 0 & f_p \end{bmatrix},$$

$$[F_A] = \frac{1}{f_a} \begin{bmatrix} 1 & (f_a - 1) & 0 & 0 \\ 0 & f_a & 0 & 0 \\ 0 & 0 & 1 & (f_a - 1) \\ 0 & 0 & 0 & f_a \end{bmatrix}, \quad [P] = \frac{1}{(1-2p)} \begin{bmatrix} -p & 0 & (1-p) & 0 \\ 0 & -p & 0 & (1-p) \\ (1-p) & 0 & -p & 0 \\ 0 & (1-p) & 0 & -p \end{bmatrix},$$

$$[A] = \frac{1}{(1-2a)} \begin{bmatrix} -a & (1-a) & 0 & 0 \\ (1-a) & -a & 0 & 0 \\ 0 & 0 & -a & (1-a) \\ 0 & 0 & (1-a) & -a \end{bmatrix},$$

where Σ is the corrected data, I' is the spin-dependent measured intensity, f_p is the flipper efficiency before the sample, f_a is the flipper efficiciy after the sample, p is the polarizer efficiency, and a is the analyzer efficiency.

Second, analyzer-reflected (I^{++},I^{-+}) and analyzer-transmitted (I^{--},I^{+-}) neutrons were simultaneously measured using an analyzer and multidetectors without a second spin flipper as shown in Fig. 1(c). These analyzer-reflected neutrons correspond to a crossed polarization, i.e., the polarizer and analyzer are configured to transmit opposite spin states. Therefore, it must be taken into account that the analyzer efficiencies should be different for analyzer-transmitted and analyzer-reflected neutrons. To do this we introduce two different efficiency values for the analyzer matrix as follows (although it is not rigorously derived theoretically):

$$[A] = \frac{1}{(1-a_1-a_2)} \times \begin{bmatrix} -a_1 & (1-a_2) & 0 & 0 \\ (1-a_1) & -a_2 & 0 & 0 \\ 0 & 0 & -a_1 & (1-a_2) \\ 0 & 0 & (1-a_1) & -a_2 \end{bmatrix}.$$

Two types of standard samples must be required for the correction. The first standard sample is four spin-dependent direct beam count rates ($I_1^{\pm\pm}$, $I_1^{\pm\mp}$) without a sample. In this measurement, two spin flippers were used. This give us two flipper efficiencies f_P and f_A and a polarizer-analyzer polarization product ϕ:

$$\phi = (2p-1)(2a-1) = \frac{(I_1^{--}-I_1^{+-})(I_1^{--}-I_1^{-+})}{I_1^{++}\times I_1^{--} - I_1^{+-}\times I_1^{-+}},$$

$$f_p = \frac{I_1^{++}-I_1^{+-}-I_1^{-+}+I_1^{--}}{2(I_1^{--}-I_1^{-+})},$$

$$f_a = \frac{I_1^{++}-I_1^{+-}-I_1^{-+}+I_1^{--}}{2(I_1^{--}-I_1^{+-})}.$$

The other standard sample is four spin-dependent beam counts rates ($I_2^{\pm\pm}$ and $I_2^{\pm\mp}$) measured at magnetic saturation. In this case we measured four spin-dependent count rates using a crossed polarization method without the second spin flipper after the sample. The unique p value is given by the following equation and then the analyzer efficiency a can be determined from p and ϕ:

$$(2p-1)^2 = \phi\left(\frac{(1-2f_a)I_2^{--}+(2f_a-1)I_2^{+-}-I_2^{-+}+I_2^{++}}{(1-2f_p)I_2^{--}+(2f_p-1)I_2^{-+}-I_2^{+-}+I_2^{++}}\right),$$

$$(2a-1) = \frac{\phi}{(2p-1)}.$$

Polarizer and analyzer efficiencies were calculated for each sample under magnetic saturation conditions.

*kykim3060@kaeri.re.kr
†cyyou@inha.ac.kr

[1] J. Nogués and I. K. Schuller, J. Magn. Magn. Mater. **192**, 203 (1999).
[2] C. Leighton, J. Nogués, B. J. Jönsson-Åkerman, and Ivan K. Schuller, Phys. Rev. Lett. **84**, 3466 (2000).
[3] M. R. Fitzsimmons, P. Yashar, C. Leighton, I. K. Schuller, J. Nogués, C. F. Majkrzak, and J. A. Dura, Phys. Rev. Lett. **84**, 3986 (2000).
[4] Z.-P. Li, O. Petracic, R. Morales, J. Olamit, X. Batlle, K. Liu, and I. K. Schuller, Phys. Rev. Lett. **96**, 217205 (2006).
[5] X. P. Qiu, D. Z. Yang, S. M. Zhou, R. Chantrell, K. O'Grady, U. Nowak, J. Du, X. J. Bai, and L. Sun, Phys. Rev. Lett. **101**, 147207 (2008).
[6] H.-C. Choi, C.-Y. You, K.-Y. Kim, J.-S. Lee, J.-H. Shim, and D.-H. Kim, Phys. Rev. B **81**, 224410 (2010).
[7] B. Dieny, V. S. Speriosu, S. S. P. Parkin, B. A. Gurney, D. R. Wilhoit, and D. Mauri, Phys. Rev. B **43**, 1297 (1991).
[8] S. A. Wolf, D. D. Awschalom, R. A. Buhrman, J. M. Daughton, S. von Molnár, M. L. Roukes, A. Y. Chtchelkanova, and D. M. Treger, Science **294**, 1488 (2001).
[9] N. J. Gökemeijer, T. Ambrose, and C. L. Chien, Phys. Rev. Lett. **79**, 4270 (1997).
[10] Luc Thomas, Andrew J. Kellock, and Stuart S. P. Parkin, J. Appl. Phys. **87**, 5061 (2000).
[11] Y.-Y. Song, D.-H. Kim, S.-C. Yu, Petr. D. Kim, I. A. Turpanov, L. A. Lee, A. E. Buzmakov, and K.-W. Lee, J. Appl. Phys. **103**, 07C112 (2008).
[12] M. Gierlings, J. Prandolini, M. Gruyters, T. Funk, D. Riegel, and W. D. Brewer, Eur. Phys. J. B **45**, 137 (2005).
[13] F. Garcia, J. Sort, B. Rodmacq, S. Auffret, and B. Dieny, Appl. Phys. Lett. **83**, 3537 (2003).
[14] T. Mewes, B. F. P. Roos, S. O. Demokritov, and B. Hillebrands, J. Appl. Phys. **87**, 5064 (2000).
[15] W. Kuch, L. I. Chelaru, F. Offi, J. Wang, M. Kotsugi, and J. Kirschner, Nature Mater. **5**, 128 (2006).
[16] F. Y. Yang and C. L. Chien, Phys. Rev. Lett. **85**, 2597 (2000).
[17] D. N. H. Nam, W. Chen, K. G. West, D. M. Kirkwood, J. Lu, and S. A. Wolf, Appl. Phys. Lett. **93**, 152504 (2008).
[18] R. Morales, Zhi-Pan Li, J. Olamit, Kai Liu, J. M. Alameda, and Ivan K. Schuller, Phys. Rev. Lett. **102**, 097201 (2009).
[19] R. Nakatani, Katsumi Hoshino, Shin Noguchi, and Yutaka Sugita, Jpn. J. Appl. Phys. **33**, 133 (1994).
[20] K.-Y. Kim, H.-C. Choi, C.-Y. You, and J.-S. Lee, J. Magnetics **13**, 97 (2008).
[21] C. Daboo, J. A. C. Bland, R. J. Hicken, A. J. R. Ives, M. J. Baird, and M. J. Walker, Phys. Rev. B **47**, 11852 (1993).
[22] Z. Y. Liu and S. Adenwalla, J. Appl. Phys. **93**, 3422 (2003).
[23] K.-Y. Kim, J.-W Kim, H.-C. Choi, C.-Y. You, S.-C. Shin, and J.-S. Lee, J. Magnetics **14**, 36 (2009).

[24] *Ultrathin Magnetic Structures*, edited by J. A. C. Bland and B. Heinrich (Springer, Berlin, 2005), Chap. 7, pp. 232–284.
[25] C. F. Majkrzak, K. V. O'Donovan, and N. F. Berk, in *Neutron Scattering from Magnetic Materials*, edited by Tapan Chatterji (Elsevier, Amsterdam, 2006).
[26] F. Mezei, Golub, F. Klose, and H. Toews, Physica B **213-214**, 898 (1995).
[27] J. Demeter, J. Meersschaut, F. Almeida, S. Brems, C. Van Haesendonck, A. Teichert, R. Steitz, K. Temst, and A. Vantomme, Appl. Phys. Lett. **96**, 132503 (2010).
[28] M. Ali, C. H. Marrows, and B. J. Hickey, Phys. Rev. B **67**, 172405 (2003).
[29] J. Nogués, J. Sort, V. Langlais, V. Skumryev, S. Suriñach, J. S. Muñoz, and M. D. Baró, Phys. Rep. **422**, 65 (2005).
[30] I. N. Krivorotov, C. Leighton, J. Nogués, Ivan K. Schuller, and E. D. Dahlberg, Phys. Rev. B **65**, 100402 (2002).
[31] E. Girgis, R. D. Portugal, H. Loosvelt, M. J. Van Bael, I. Gordon, M. Malfait, K. Temst, C. Van Haesendonck, L. H. A. Leunissen, and R. Jonckheere, Phys. Rev. Lett. **91**, 187202 (2003).
[32] Johannes Eisenmenger, Zhi-Pan Li, Waldemar A. A. Macedo, and Ivan K. Schuller, Phys. Rev. Lett. **94**, 057203 (2005).
[33] R. M. Osgood III, S. D. Bader, B. M. Clemens, R. L. White, and H. Matsuyama, J. Magn. Magn. Mater. **182**, 297 (1998).
[34] T. Mewes, H. Nembach, M. Rickart, and B. Hillebrands, J. Appl. Phys. **95**, 5324 (2004).
[35] A. R. Wildes, Neutron News **17**, 17 (2006).